



**HAL**  
open science

## Custom 3D Printed Spatial Atomic Layer Deposition Manifold for the Coating of Tubular Membranes

Fidel Toldra-Reig, Clément Lausecker, Matthieu Weber, Mikhael Bechelany,  
David Muñoz-Rojas

► **To cite this version:**

Fidel Toldra-Reig, Clément Lausecker, Matthieu Weber, Mikhael Bechelany, David Muñoz-Rojas. Custom 3D Printed Spatial Atomic Layer Deposition Manifold for the Coating of Tubular Membranes. *ACS Sustainable Chemistry & Engineering*, 2022, 10 (43), pp.14112-14118. 10.1021/acssuschemeng.2c04424 . hal-03852184

**HAL Id: hal-03852184**

**<https://hal.umontpellier.fr/hal-03852184>**

Submitted on 14 Nov 2022

**HAL** is a multi-disciplinary open access archive for the deposit and dissemination of scientific research documents, whether they are published or not. The documents may come from teaching and research institutions in France or abroad, or from public or private research centers.

L'archive ouverte pluridisciplinaire **HAL**, est destinée au dépôt et à la diffusion de documents scientifiques de niveau recherche, publiés ou non, émanant des établissements d'enseignement et de recherche français ou étrangers, des laboratoires publics ou privés.

# Custom 3D Printed Spatial Atomic Layer Deposition Manifold for the Coating of Tubular Membranes

*Fidel Toldra-Reig<sup>a,†,\*</sup>, Clément Lausecker<sup>a,b</sup>, Matthieu Weber<sup>a</sup>, Mikhael Bechelany<sup>b</sup> and David  
Muñoz-Rojas<sup>a,\*\*</sup>*

<sup>a</sup> Univ. Grenoble Alpes, CNRS, Grenoble INP, LMGP, F-38000 Grenoble, France

<sup>b</sup> Institut Européen des Membranes, IEM, UMR-5635, Univ. Montpellier, CNRS, ENSCM, Place  
Eugène Bataillon 34095 Montpellier cedex 5, France

## **Abstract**

The development of highly efficient membranes represents a great opportunity to significantly reduce the environmental impacts of human activities through gas separation and water filtration, and are also very attractive for process intensification when coupled to existing industrial processes. Tubular membranes have higher modularity, better pressure resistance, and they offer easier sealing than their flat counterparts. The ability to deposit thin films on their surface is crucial to optimize their chemical and physical properties. However, the deposition of thin films on tubular membrane supports with conventional vacuum-based deposition techniques is relatively complex, slow and costly. In this work the versatility of spatial atomic layer deposition (SALD) and 3D printing technologies has been combined to design and fabricate a custom SALD manifold for coating tubular substrates. SALD is a scalable deposition technique, offering high-throughput at atmospheric pressure and thus can be advantageously employed to coat tubular membranes, enabling high quality thin films to be deposited at the nanoscale considerably faster than with other conventional techniques. Computational fluid dynamics (CFD) calculations by means of COMSOL Multiphysics have been used to optimize this innovative SALD gas manifold. The proof-of-concept of the new SALD manifold has been validated through successful ZnO thin film depositions performed on tubular Cu foils and porous Al<sub>2</sub>O<sub>3</sub> tubular membrane supports, demonstrating the capability of SALD to achieve high-throughput depositions on non-planar, complex

25 substrates. These results open prospects for the interface engineering of membranes or electrolyzers,  
26 where precise coatings of tubular surfaces are needed.

## 27 **Keywords**

28 Inorganic membrane, Spatial Atomic Layer Deposition, 3D printing, tubular substrates, interface  
29 engineering

30

## 31 **1. Introduction**

32 The development of highly efficient membranes has become of central interest for the energy sector  
33 and the chemical industry, as the efficient separation of species represents a valuable strategy to reduce  
34 cost, energy, and environmental impact of many processes<sup>1,2</sup> or to reduce the impact of human activities  
35 by elimination of pollutants in wastewater and contaminated air. One example of current membrane energy  
36 application is the membrane-assisted separation of hydrogen for its use as energy carrier<sup>3-8</sup>, which is  
37 expected to be fundamental for the forthcoming shift to carbon-neutral societies. Coupling membranes to  
38 chemical industry is a key strategy for intensification of processes such as Fischer-Tropsch, aromatization,  
39 de/hydrogenation, reforming<sup>9-12</sup> and membrane reactors in general<sup>13</sup>.

40 The separation processes are achieved by enabling species/molecules to pass through the membrane  
41 as a result of a driving force. Most transport processes take place because of a difference in chemical  
42 potential (pressure and concentration contribute to the chemical potential). Depending on their  
43 architecture, membranes achieve fluid separation through either i) solution-diffusion, if a dense film of  
44 the appropriate material is used, or ii) molecular sieving, for appropriate porous films. In particular,  
45 tubular-shaped membranes are appealing to industry since they offer strong adaptability, easier sealing,  
46 high-pressure resistance and higher modularity than their planar counterparts. Such membranes can be  
47 prepared by dip-coating or spray-coating of tubular supports by sol-gel routes (plus spin coating or screen  
48 printing for planar membranes), but the precise control of chemical and physical properties of both dense  
49 and porous membranes (i.e., thickness, surface composition, pore size, etc.) is still a key challenge for  
50 membrane producers<sup>1,2</sup>. Thus, thin films are highly attractive for the coating of dense membranes, as it

51 decreases the amount of material required (especially for expensive or scarce elements) while improving  
52 the permeability. In addition, thin film techniques can enable a precise control of the pore size for porous  
53 membranes.

54 Among thin film deposition techniques enabling tubular coatings, physical vapor deposition (PVD)  
55 techniques have a low energy-efficiency and spinning systems are required (including heating elements)  
56 which increase the complexity and/or cost. Electrodeposition and solvothermal approaches can be used  
57 for the deposition of metals and simpler oxides with lower use of consumables and at lower cost. However,  
58 these approaches require more steps, yield thicker layers and there are also several concerns from the  
59 health, safety and environmental points of view <sup>1</sup>>. As recently reviewed, chemical vapor deposition  
60 (CVD) techniques such as atomic layer deposition (ALD) are extremely valuable for membrane science  
61 and have been tested for many applications, including gas separation and water filtration, biosensing and  
62 catalysis <sup>15-17</sup>. ALD is based on the sequential use of surface-limited, self-terminating chemical reactions  
63 that take place in a cycle-wise fashion, thus allowing to prepare conformal and high quality films at the  
64 nanoscale on complex substrates and at low temperatures <sup>18-20</sup>. ALD has traditionally been a vacuum-  
65 based technique requiring the use of relatively costly reactors and pumping systems. Spatial atomic layer  
66 deposition (SALD) is a branch of conventional ALD, in which the precursors are continuously injected  
67 in different locations of the reactor, being separated by a flow of inert gas. This technique is able to reach  
68 faster growth rates than conventional ALD and can be performed at atmospheric pressure and in the open  
69 air (i.e. without deposition chamber) <sup>21,22</sup>. This does not compromise the deposition of high quality  
70 materials, even on high-aspect -ratio substrates, with precise thickness control, high uniformity and  
71 excellent conformality <sup>23-25</sup>.

72 SALD can indeed be implemented in different ways <sup>2</sup>>. This work is based on the close-proximity  
73 manifold approach <sup>27,28</sup>, where the reactants are distributed along adjacent channels and separated by inert  
74 gas and exhausts channels <sup>29</sup>. The close proximity of the substrate to the head then ensures the efficient  
75 separation of the reactants. The movement of the substrate exposes the surface to the different reactants,  
76 therefore reproducing the layer-by-layer growth of conventional ALD. This SALD approach is

77 particularly versatile since it can be easily tuned by simply modifying the manifold injector. For instance,  
78 we have shown that 3D printing can be used to customize close-proximity SALD manifolds in different  
79 materials, opening up a large span of possibilities <sup>30,31</sup>.

80 However, SALD has been only used to coat planar substrates such as wafers, glasses, or flat  
81 polymeric substrates so far. Porous materials or high-aspect-ratio features have also been coated, but the  
82 macroscopic nature of these samples is a flat substrate. A notable exception has been reported van  
83 Ommen's group where the coating of nanoparticles was enabled by implementing a SALD system in a  
84 fluidized reactor <sup>32</sup>. In this work, we take advantage of 3D printing to design a gas manifold specifically  
85 tailored for tubular supports. To demonstrate the feasibility to perform SALD on such tubular surfaces,  
86 ZnO layers have been deposited on Cu foils wrapped around tubular supports and on Al<sub>2</sub>O<sub>3</sub> tubular porous  
87 membrane substrates. This work is a new versatile way of printing functional devices to extend the current  
88 potential of SALD<sup>33-35</sup> to membrane applications, opening a new avenue in the field for coating complex  
89 substrates with functional materials.

## 90 **2. Materials and Methods**

### 91 *2.1. SALD of ZnO on tubular supports*

92 The gas manifold was elaborated through computer-aided design (CAD) in Solid Edge and 3D printed  
93 by stereolithography (FORM2, Formlabs) with Clear V4 (Formlabs). Supports and resin leftovers were  
94 carefully removed and the 3D-piece was cleaned with isopropanol (<99.8% purity, Honeywell) and  
95 cautiously dried prior to SALD deposition. Simulations of the gas pressure distribution among the  
96 prechambers and gas outlet channels within the SALD gas manifolds were performed in COMSOL  
97 Multiphysics software using the CFD module.

98 ZnO was deposited at room temperature using a custom-made atmospheric pressure SALD system  
99 <sup>3></sup>. Two substrates were considered : i) Cu foils (3M) wrapped around 3D printed polymer tubes of 1 cm  
100 diameter, and ii) commercial Al<sub>2</sub>O<sub>3</sub> porous tubular membranes (50 nm pore size diameter, Atech  
101 Innovations GmbH) of 1 cm outer diameter. Diethylzinc (DEZ, Zn(C<sub>2</sub>H<sub>5</sub>)<sub>2</sub>, Sigma Aldrich) and water

102 (H<sub>2</sub>O) were used as metal precursor and coreactant respectively. Nitrogen (99.995%, AirLiquide) was  
103 used both as a carrying gas in precursor lines and as barrier gas in dedicated lines separating DEZ and  
104 water flows. The precursors were carried from the bubblers to the gas manifold by flowing 15 and 90  
105 sccm of nitrogen through the DEZ and water bubblers, and were subsequently diluted with 135 and 210  
106 sccm of additional nitrogen, respectively. The total nitrogen flowrate used as barrier gas was 600 sccm.

## 107 *2.2. Characterization Techniques*

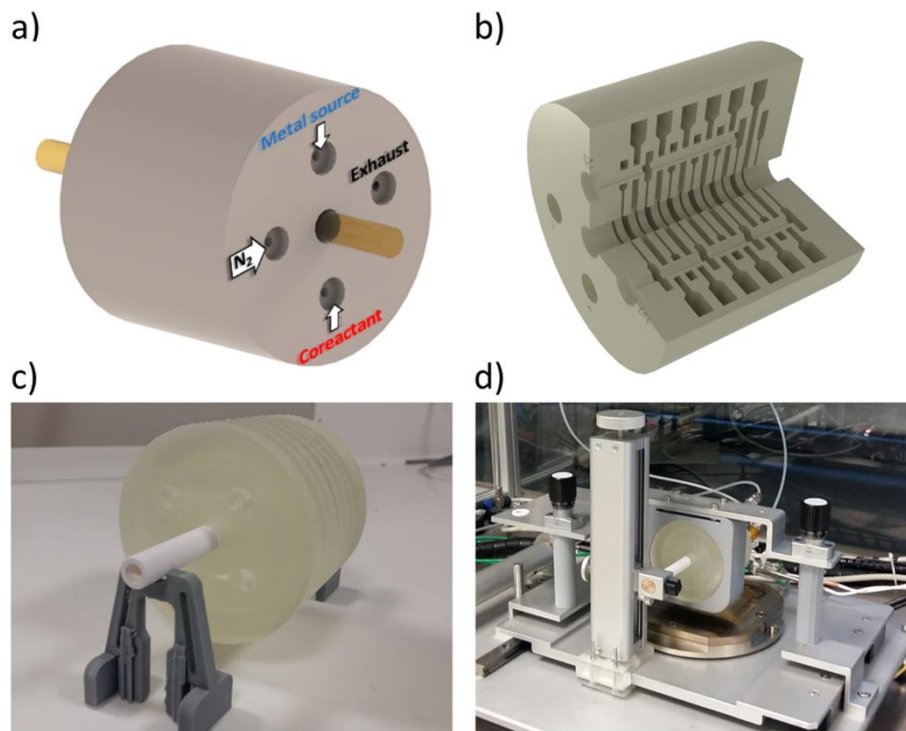
108 The morphology of the deposited ZnO thin films was investigated by field-emission scanning electron  
109 microscopy (FESEM) using a Zeiss Gemini 300 field-emission-gun scanning electron microscope.  
110 FESEM energy-dispersive X-ray spectroscopy (EDS) spectra were recorded using a Bruker X-ray  
111 detector incorporated in the Zeiss Gemini 300 field-emission-gun scanning electron microscope operating  
112 at 15 kV. X-ray diffraction (XRD) patterns were collected with a Rigaku SmartLab diffractometer  
113 equipped with a rotating Cu anode operating at 9 kW (45 kV and 200 mA) from which the Cu K $\alpha$ <sub>1</sub>  
114 radiation was used. The  $\theta$ -2 $\theta$  scans were performed in the standard Bragg–Brentano configuration with a  
115 step of 0.1° and a speed of 0.3° s<sup>-1</sup> using parallel beams (divergence less than 0.05°). The ZnO and  $\alpha$ -  
116 Al<sub>2</sub>O<sub>3</sub> diffraction peaks were indexed according to the ICDD 00-036-145 and 00-046-1212 files,  
117 respectively.

## 118 **3. Results and Discussion**

### 119 *3.1. Design and fabrication of the tubular gas manifold*

120 The possibility to 3D print gas manifolds enable the integration of gas distribution and separation  
121 circuits into the body as shown in our group previously<sup>30,31</sup>. In this work, we take further advantage of  
122 these capabilities to design a gas manifold for deposition on tubular substrates based in the same close-  
123 proximity technology. More specifically, a cylindric gas manifold dedicated to the SALD of tubular  
124 surfaces was fabricated through CAD and 3D printing, as illustrated in Fig. 1. The gas manifold contains  
125 four external connections, as revealed by Fig. 1a, being the inlets for metal precursor, coreactant, inert  
126 gas, and the exhaust outlet. In this configuration, the tubular substrate is introduced in the central

127 cylindrical hole of the gas manifold and moves back and forth during deposition to ensure the exposition  
128 of its surface to the different gases. The hole diameter can be easily adjusted to the substrate diameter in  
129 order to have a controlled gap in the range of 50-200  $\mu\text{m}$  between the substrate surface and the gas outlets.  
130 Furthermore, both inlet and outlet channels connect to individual concentric prechambers located within  
131 the the bulk of the gas manifold as detailed in the cross-section view shown in Fig. 1b. These prechambers  
132 have a concentric outlet channel facing the substrate to ensure the exposure of the substrate to the gases  
133 or to extract them.

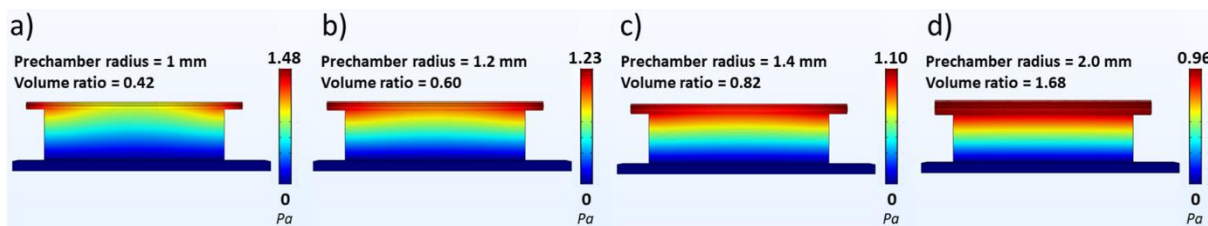


134

135 **Fig. 1.** (a) Scheme of the cylindrical SALD manifold designed to coat tubular substrates, (b) detailed  
136 cross-section view of the design, (c) printed version of the gas manifold, and (d) integration into the  
137 custom-made SALD system.

138 The concentric prechambers are required to ensure a good homogeneization of the gas pressure and  
139 its proper distribution through the outlet channel. An inappropriate design would lead to inhomogeneous  
140 deposition with unexposed areas on the tubular substrate <sup>35</sup>. Prior to the design, COMSOL Multiphysics  
141 simulations using the CFD module were performed to find adequate ratios between the prechamber and  
142 the channel outlet volumes offering optimal gas pressure distributions, whose results are summarized in  
143 Fig. 2. The study was performed on an individual 3D channel of a standard SALD gas manifold <sup>39</sup> for the

144 sake of time and hardware requirements. There are two inlets in each side of the prechamber, and one  
 145 outlet at the bottom of the channel where the substrate is located. As stated before, the flow and pressure  
 146 through the prechamber and channel outlet are evaluated to check the size of prechamber yielding a good  
 147 homogeneity of the gas, i.e. a constant flow front reaching the substrate surface. **Otherwise, preferential**  
 148 **pathways, extended regions with different gas speeds, or dead zones where no gas flow occur can be**  
 149 **generated, leading to an innacurate gas distribution and a lack of homogeneity in the deposition.** To do  
 150 so, the channel outlet volume was kept constant (with channel dimensions fixed at  $50 \times 15 \times 0.5 \text{ mm}^3$ )  
 151 and the radius of the prechamber was varied from 1 to 2 mm. Moreover, a constant flowrate of 100 mL/min  
 152 was applied to both prechamber inlets. The results reveal that a small prechamber volume (i.e. with a  
 153 radius of 1 mm, Fig. 2a) should be avoided as it produces very inhomogeneous gas flow distribution along  
 154 the outlet channel. The homogeneity of the gas is drastically improved when increasing the prechamber  
 155 volume (i.e. when increasing its radius above 1 mm, Fig. 2b-d), a minimum radii between 1.4 and 2 mm  
 156 is required to ensure good homogeneization (Fig. 2c,d). Therefore, as a general rule, a prechamber/channel  
 157 outlet volume ratio of at least 0.8 should be respected for the design of the cylindrical SALD manifold.



158  
 159 **Fig. 2.** CFD calculations made with COMSOL Multiphysics, where the fluid distribution is assessed along  
 160 an outlet channel for varying prechamber radii of (a) 1 mm, (b) 1.2 mm, (c) 1.4 mm, and (d) 2.0 mm. The  
 161 corresponding prechamber/channel outlet volume ratios are also indicated.

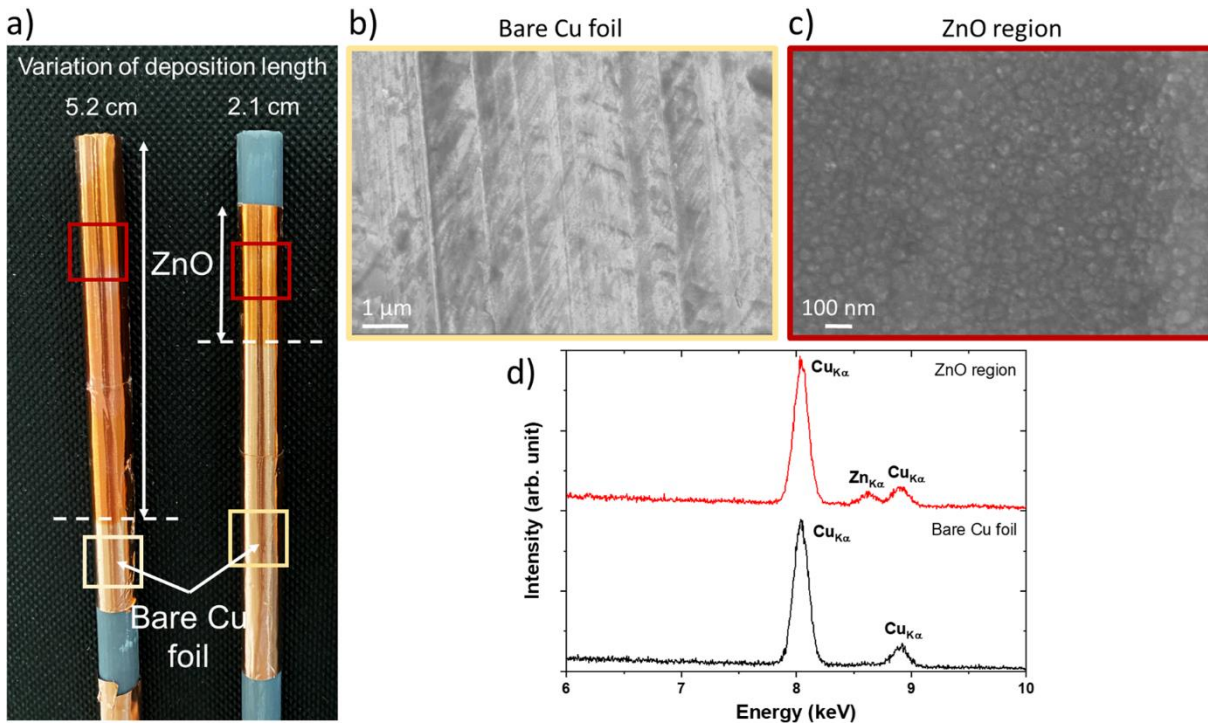
162 The concentric nature of the gas manifold also adds some complexity to the 3D printing process.  
 163 Indeed, to guarantee its feasibility, temporary supports must be printed in the central hole where the  
 164 substrate is to be placed. However, the smoothness of this internal surface is capital for the deposition  
 165 process ensuring an even distribution of the flow. The supports were thus removed carefully and the  
 166 internal cylindrical surface was polished with fine polishing paper (1200) to smooth the surface.  
 167 Additionnally, a thorough cleaning of the inner channels with isopropanol followed by a drying process



168 must be done to avoid any loss of shape or blockage of the outer channels due to resin or liquid  
169 accumulation. A Dino-Lite RK-10 holder with integrated z-axis controller is used as a sample holder to  
170 accurately control the height of the tubular sample, providing precise alignment with the gas manifold.  
171 The sample holder is secured by a 3D printed home-made piece to the SALD moving plate, tightening the  
172 tubular sample at its position at the center of the gas manifold and ensuring an appropriate gap with gas  
173 outlets (Fig. 1d).

### 174 3.2. SALD of ZnO on tubular substrates

175 A first validation of the gas manifold design and integration into the SALD system was performed  
176 using 3D printed tubes of 1 cm diameter wrapped with Cu foils as tubular substrates. Cu foils permit the  
177 visual identification of the deposition through their change of contrast, and they can be easily unwrapped  
178 from the 3D printed tubes for later characterization in SEM. ZnO was chosen because it is a school-case  
179 ALD material and because the group has extensive expertise in its deposition <sup>36,39</sup>. Additionally,  
180 amorphous ZnO can be grown at room temperature facilitating the operational validation of the gas  
181 manifold. Standard SALD conditions previously reported for ZnO deposition (<sup>36,39</sup> on planar substrates)  
182 were tested successfully as depicted in Fig. 3a. The deposition distance (i.e. the amplitude of the substrate  
183 displacement) was varied and the related changes of contrast observed confirm that the deposition is  
184 taking place in the desired region, which can thus be typically controlled in the range of a few centimeters.  
185 Moreover, FESEM observations of the Cu foils (Fig. 3b,c) confirm the growth of a ZnO thin film in the  
186 region exposed to precursors, while no ZnO is observed in the pristine region. The ZnO layer covers the  
187 whole surface exposed, with no apparent change between regions. The deposition of ZnO is further  
188 confirmed by FESEM-EDS analyses (Fig. 3d), where a significant signal associated to the  $Zn_{K\alpha}$  energy  
189 transition is observed at around 8.6 keV in the region exposed to precursors, while this signal is absent on  
190 the pristine Cu foil.

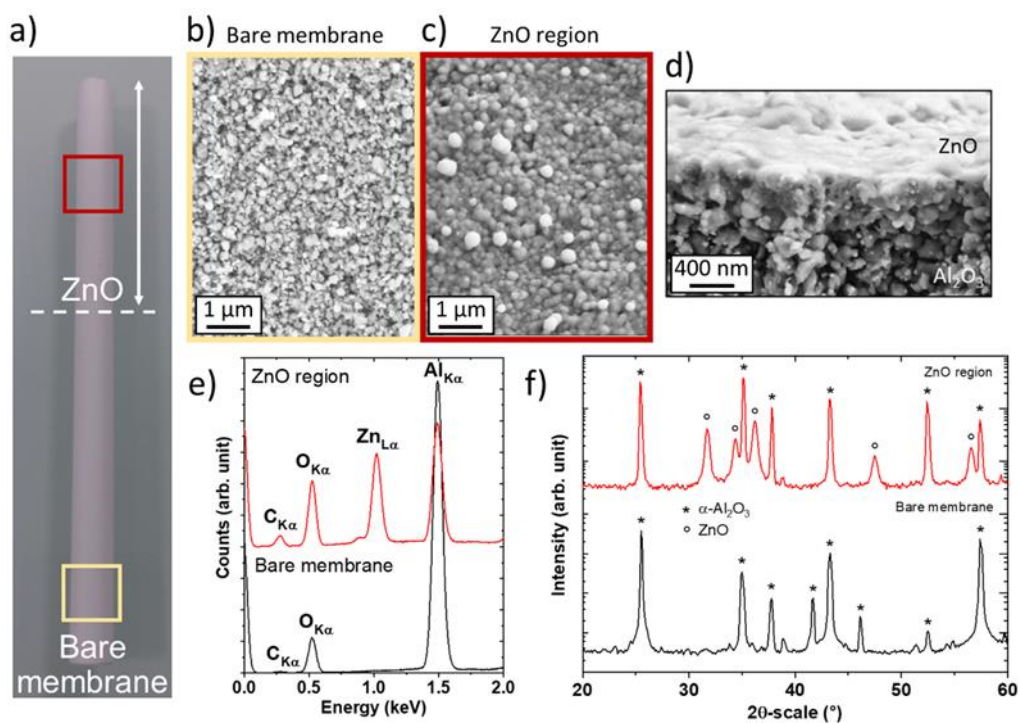


191

192 **Fig. 3.** (a) Cu foils with ZnO depositions along variable lengths. Top-view FESEM images of (b) a bare  
 193 Cu foil and of (c) a Cu foil with ZnO deposition. (d) Corresponding FESEM-EDS spectra.

194 In a second step, we aimed to confirm the potential of this new approach for the surface engineering  
 195 of membrane supports by using the 3D printed gas manifold to perform SALD on porous  $\alpha$ -Al<sub>2</sub>O<sub>3</sub> tubular  
 196 ceramic supports (50 nm pore size), such as the one presented in Fig. 4a. The equivalent to 1000  
 197 conventional ALD cycles were used for deposition of ZnO. FESEM observations revealed the deposition  
 198 of a ZnO thin layer with an estimated thickness of 400 nm, corresponding to a growth rate of 4 Å/cycle  
 199 (Fig. 4b,c). It can be noted that the growth rate is higher than what is typically expected for an ALD  
 200 process, implying a major CVD contribution during the ZnO deposition. Indeed, the possibility to grow  
 201 both in CVD and ALD mode is one of the advantages offered by close-proximity SALD based on  
 202 manifold heads. Deposition in SCVD mode has been used in the past and, for surfaces with no complex  
 203 or high-aspect-ratio features, homogenous films can be obtained with GPC values larger than for the  
 204 equivalent ALD process. The optimization of the tubular head presented here is possible for the cases  
 205 when ALD conditions are required. These optimizations will involve the adjustment of parameters such  
 206 as the flow rates, the gap between the gas manifold and the sample surface, the channel width and  
 207 separation, and the sample movement speed. A strong associated signal of the Zn<sub>Lα</sub> energy transition at

208 around 1.0 eV is further measured from FESEM-EDS characterizations in areas exposed to the chemical  
 209 precursors (otherwise absent on the bare membrane), confirming the ZnO chemical nature of the thin layer  
 210 (Fig. 4d). Moreover, different membrane pieces were characterized by XRD to gain more insights on their  
 211 structural properties. To ensure good crystallization of the ZnO thin film, the samples were annealed at  
 212 500 °C during 1 h. The obtained XRD patterns in the deposited region, shown in Fig. 4e, clearly reveal  
 213 the presence of several diffraction peaks associated to wurtzite ZnO, while only diffraction peaks  
 214 associated to  $\alpha$ -Al<sub>2</sub>O<sub>3</sub> are present on the bare membrane. These results demonstrate the great potential of  
 215 SALD for the deposition of high quality thin films on complex substrates such as tubular membrane  
 216 supports. Additionally, the repeatability of the depositions and reuse of the gas manifold can be typically  
 217 achieved through a proper alignment of the sample using the level adjuster described previously and a  
 218 thorough gas manifold maintenance (cleaning with 5% nitric acid solution, rinsing with isopropanol and  
 219 drying), respectively.



220  
 221 **Fig. 4.** (a) Tubular membrane support after ZnO deposition. (b,c) Top-view FESEM images of the  
 222 membrane (b) without and (c) with ZnO deposition. (d) High-magnification cross-section view of the  
 223 ZnO thin film. (e) Corresponding FESEM-EDS spectra, and (f) XRD patterns of membrane pieces without  
 224 and with ZnO deposition after annealing at 500 °C.

### 225 3.3 Perspectives

226 The present work shows a proof of concept reporting the coating of tubular membranes by an an  
227 open-air technique (SALD) which is attractive for interface engineering because of both conformal coating  
228 and excellent thickness control. For example, some ALD-prepared materials such as palladium or metal-  
229 organic frameworks (MOFs) are particularly relevant for the fabrication of separation membranes <sup>40,41</sup>. It  
230 is worth noting that thin films such as ZnO can be subsequently converted to a MOF by hydrothermal  
231 techniques. Heating elements can also be easily incorporated to the system to enable the deposition of  
232 materials not available at room temperature.

233 Capability to deposit dense thin layers over porous tubular supports enables the use of SALD for the  
234 coating of dense membranes as well as other electrochemical devices such as fuel cells/electrolyzers or  
235 electrochemical membrane reactors with tailored electrodes <sup>42-51</sup>, where the gas separation occurs by  
236 adsorption and diffusion through the thin layer. Different ionic and protonic materials comprising more  
237 complex oxides or metals have already been deposited by ALD <sup>52-60</sup>, and their addition to the SALD  
238 palette for both planar and tubular depositions would be appealing for various industrial applications.  
239 Moreover, the gas manifold design could be adapted for the coating of other types of non-planar  
240 substrates, which could be used in various applications such as free-form electronics <sup>61</sup> or for curved  
241 lenses and mirrors fabrication <sup>62,63</sup>.

242 SALD gas manifolds can be also modular (coupling several manifolds in series) enlarging the  
243 deposition area. This can be also used to tailor deposition i.e. different modules with alternating materials  
244 can be used to have multimaterial and multifunctional devices.

## 245 4. Conclusions

246 In this work, we successfully performed thin film deposition on tubular substrates using the  
247 atmospheric pressure SALD technique in the open-air close-proximity approach. Using computational  
248 fluid dynamics calculations, an innovative SALD gas manifold has been designed and fabricated thanks  
249 to the versatility offered by 3D printing. The custom gas manifold has been designed to deliver a  
250 concentric homogeneous precursor gas outflow covering the whole surface of tubular substrates. The

251 relations between the different volumes within the gas manifolds has been evaluated by means of COMSOL  
252 Multiphysics. Using DEZ and water as precursors, the design of the gas manifold has been validated by  
253 depositing ZnO onto Cu foils and porous alumina tubular supports. The successful depositions show the  
254 high potential of SALD for the engineering of membrane interfaces. Further optimization will result in  
255 heads in which the ALD and CVD mode can be precisely controlled by adjusting the different flows.  
256 These results open the door to the high-throughput fabrication of both dense and porous tubular  
257 membranes of various materials by SALD. This approach can be further adapted to the preparation of  
258 other nanomaterials as well as to other substrate geometries, widening the field of applications of SALD  
259 on complex surfaces.

## 260 AUTHOR INFORMATION

### 261 **Corresponding Author**

262 \* Corresponding author 1. *E-mail address:* fitolrei@itq.upv.es (D. Fidel Toldrá Reig)

263 \*\* Corresponding author 2. *E-mail address:* [david.munoz-rojas@grenoble-inp.fr](mailto:david.munoz-rojas@grenoble-inp.fr) (D. Muñoz-Rojas)

### 264 **Present Addresses**

265 † Current Address: Instituto de Tecnología Química (CSIC-UPV), Universitat Politècnica de València,  
266 Camino de vera s/n, 46022, Valencia, Spain

### 267 **Author Contributions**

268 The manuscript was written through contributions of all authors. All authors have given approval to the  
269 final version of the manuscript.

### 270 **Funding Sources**

271 This work was supported by the French Research National Agency through the project ALD4MEM (ANR  
272 ANR-20-CE09-0008).

### 273 **Acknowledgments**

274 The authors thank the French Research National Agency for funding (ANR ANR-20-CE09-0008) and  
275 Hervé Roussel from LMGP for the XRD characterizations.

- 277 (1) Zydney, A. L. *Membrane Handbook*, Winston Ho, W. S.; Sirkar, K.K.; Reinhold, V.N.; Eds.; John  
278 Wiley & Sons, Ltd, New York, 1992, AIChE J. 41 **1995**, 2343–2344.. DOI:  
279 10.1002/AIC.690411024.
- 280 (2) *Comprehensive Membrane Science and Engineering (Second Edition)* Drioli, E.; Giorno, L.,  
281 Fontananova, E., Eds. ; Elsevier: London, **2017**.
- 282 (3) Ivanova, M. E.; Escolástico, S.; Balaguer, M.; Palisaitis, J.; Sohn, Y. J.; Meulenber, W. A.;  
283 Guillon, O.; Mayer, J.; Serra, J. M. Hydrogen Separation through Tailored Dual Phase Membranes  
284 with Nominal Composition BaCe<sub>0.8</sub>Eu<sub>0.2</sub>O<sub>3-δ</sub>:Ce<sub>0.8</sub>Y<sub>0.2</sub>O<sub>2-δ</sub> at Intermediate Temperatures.  
285 *Nat. Publ. Gr.* **2016**, 6, 34773. DOI: 10.1038/srep34773.
- 286 (4) Iwahara, H.; Asakura, Y.; Katahira, K.; Tanaka, M. Prospect of Hydrogen Technology Using  
287 Proton-Conducting Ceramics. In *Solid State Ionics* **2004**, 168, 299–310. DOI:  
288 10.1016/j.ssi.2003.03.001.
- 289 (5) Gallucci, F.; Medrano, J. A.; Fernandez, E.; Melendez, J.; Van Sint Annaland, M.; Pacheco-  
290 Tanaka, D. A. Advances on High Temperature Pd-Based Membranes and Membrane Reactors for  
291 Hydrogen Purification and Production. *Journal of Membrane Science and Research.* **2017**, 3, 142–  
292 156. DOI: 10.22079/jmsr.2017.23644.
- 293 (6) Jeong, S. W.; Yamaguchi, T.; Okamoto, M.; Zhu, C.; Habazaki, H.; Nagayama, M.; Aoki, Y.  
294 Proton Pumping Boosts Energy Conversion in Hydrogen-Permeable Metal-Supported Protonic  
295 Fuel Cells. *ACS Appl. Energy Mater.* **2020**, 3 (1), 1222–1234. DOI: 10.1021/acsaem.9b02287.
- 296 (7) Meng, T.; Young, K.; Beglau, D.; Yan, S.; Zeng, P.; Cheng, M. M.-C. Hydrogenated Amorphous  
297 Silicon Thin Film Anode for Proton Conducting Batteries. *J. Power Sources* **2016**, 302, 31–38.  
298 DOI: 10.1016/J.JPOWSOUR.2015.10.045.
- 299 (8) Itoh, N.; Xu, W. .; Hara, S.; Sakaki, K. Electrochemical Coupling of Benzene Hydrogenation and  
300 Water Electrolysis. *Catal. Today* **2000**, 56 (1–3), 307–314. DOI: 10.1016/S0920-5861(99)00288-  
301 6.
- 302 (9) Serra, J. M. Electrifying Chemistry with Protonic Cells. *Nat. Energy* **2019**, 4 (3), 178–179. DOI:  
303 10.1038/s41560-019-0353-y.
- 304 (10) Escorihuela, S.; Toldra-Reig, F.; Escolástico, S.; Murciano, R.; Martínez, A.; Serra, J. M. Copper  
305 Surface-Alloying of H<sub>2</sub>-Permeable Pd-Based Membrane for Integration in Fischer–Tropsch  
306 Synthesis Reactors. *J. Memb. Sci.* **2021**, 619, 118516. DOI: 10.1016/j.memsci.2020.118516.
- 307 (11) Solís, C.; Toldra-Reig, F.; Balaguer, M.; Somacescu, S.; Garcia-Fayos, J.; Palafox, E.; Serra, J. M.  
308 Mixed Ionic–Electronic Conduction in NiFe<sub>2</sub>O<sub>4</sub>–Ce<sub>0.8</sub>Gd<sub>0.2</sub>O<sub>2-δ</sub> Nanocomposite Thin Films  
309 for Oxygen Separation. *ChemSusChem* **2018**, 11, 2818–2827. DOI: 10.1002/cssc.201800420.
- 310 (12) Malerød-Fjeld, H.; Clark, D.; Yuste-Tirados, I.; Zanón, R.; Catalán-Martinez, D.; Beeff, D.;  
311 Morejudo, S. H.; Vestre, P. K.; Norby, T.; Haugsrud, R.; Serra, J. M.; Kjølseth, C. Thermo-  
312 Electrochemical Production of Compressed Hydrogen from Methane with near-Zero Energy Loss.  
313 *Nat. Energy* **2017**, 2 (12), 923–931. DOI: 10.1038/s41560-017-0029-4.
- 314 (13) Arratibel Plazaola, A.; Pacheco Tanaka, D. A.; Van Sint Annaland, M.; Gallucci, F. Recent  
315 Advances in Pd-Based Membranes for Membrane Reactors. *Molecules* **2017**, 22, 51 DOI:  
316 10.3390/molecules22010051.
- 317 (14) Merlo, A.; Léonard, G. Magnetron Sputtering vs. Electrodeposition for Hard Chrome Coatings: A

- 318 Comparison of Environmental and Economic Performances **2021**, *14* (14), 3823. DOI:  
319 10.3390/MA14143823/S1.
- 320 (15) Weber, M.; Julbe, A.; Kim, S. S.; Bechelany, M. Atomic Layer Deposition (ALD) on Inorganic or  
321 Polymeric Membranes. *J. Appl. Phys.* **2019**, *126* (4), 041101. DOI: 10.1063/1.5103212.
- 322 (16) Weber, M.; Julbe, A.; Ayrál, A.; Miele, P.; Bechelany, M. Atomic Layer Deposition for  
323 Membranes: Basics, Challenges, and Opportunities. *Chem. Mater.* **2018**, *30* (21), 7368–7390. DOI:  
324 10.1021/acs.chemmater.8b02687.
- 325 (17) Yang, H. C.; Waldman, R. Z.; Chen, Z.; Darling, S. B. Atomic Layer Deposition for Membrane  
326 Interface Engineering. *Nanoscale*. Royal Society of Chemistry November 28, 2018, pp 20505–  
327 20513. DOI: 10.1039/c8nr08114j.
- 328 (18) George, S. M. Atomic Layer Deposition: An Overview. *Chem. Rev.* **2010**, *110* (1), 111–131. DOI:  
329 10.1021/cr900056b.
- 330 (19) Johnson, R. W.; Hultqvist, A.; Bent, S. F. A Brief Review of Atomic Layer Deposition: From  
331 Fundamentals to Applications. *Mater. Today* **2014**, *17* (5), 236–246. DOI:  
332 10.1016/j.mattod.2014.04.026.
- 333 (20) Leskelä, M.; Ritala, M. Atomic Layer Deposition (ALD): From Precursors to Thin Film Structures.  
334 *Thin Solid Films* **2002**, *409* (1), 138–146. DOI: 10.1016/S0040-6090(02)00117-7.
- 335 (21) Muñoz-Rojas, D.; Macmanus-Driscoll, J. Spatial Atmospheric Atomic Layer Deposition: A New  
336 Laboratory and Industrial Tool for Low-Cost Photovoltaics. *Materials Horizons* **2014**, *1*, 314–320.  
337 DOI: 10.1039/c3mh00136a.
- 338 (22) Muñoz-Rojas, D.; Maindrón, T.; Esteve, A.; Píallat, F.; Kools, J. C. S.; Decams, J.-M. Speeding  
339 up the Unique Assets of Atomic Layer Deposition. *Mater. Today Chem.* **2019**, *12*, 96–120. DOI:  
340 10.1016/J.MTCHEM.2018.11.013.
- 341 (23) Musselman, K. P.; Muñoz-Rojas, D.; Hoye, R. L. Z.; Sun, H.; Sahonta, S. L.; Croft, E.; Böhm, M.  
342 L.; Ducati, C.; MacManus-Driscoll, J. L. Rapid Open-Air Deposition of Uniform, Nanoscale,  
343 Functional Coatings on Nanorod Arrays. *Nanoscale Horizons* **2017**, *2* (2), 110–117. DOI:  
344 10.1039/C6NH00197A.
- 345 (24) Nguyen, V. S.; Sekkat, A.; Bellet, D.; Chichignoud, G.; Kaminski-Cachopo, A.; Muñoz-Rojas, D.;  
346 Favre, W. Open-Air, Low-Temperature Deposition of Phase Pure Cu<sub>2</sub>O Thin Films as Efficient  
347 Hole-Transporting Layers for Silicon Heterojunction Solar Cells. *J. Mater. Chem. A* **2021**, *9* (29),  
348 15968–15974. DOI: 10.1039/D1TA02931B.
- 349 (25) Nguyen, V. H.; Resende, J.; Papanastasiou, D. T.; Fontanals, N.; Jiménez, C.; Muñoz-Rojas, D.;  
350 Bellet, D. Low-Cost Fabrication of Flexible Transparent Electrodes Based on Al Doped ZnO and  
351 Silver Nanowire Nanocomposites: Impact of the Network Density †. *Nanoscale* **2019**, *11*, 12097.  
352 DOI: 10.1039/c9nr02664a.
- 353 (26) Muñoz-Rojas, D.; Huong Nguyen, V.; Masse de la Huerta, C.; Jiménez, C.; Bellet, D. Spatial  
354 Atomic Layer Deposition. In *Chemical Vapor Deposition for Nanotechnology*; IntechOpen, **2019**.  
355 DOI: 10.5772/intechopen.82439.
- 356 (27) Levy, D. H.; Freeman, D.; Nelson, S. F.; Cowdery-Corvan, P. J.; Irving, L. M. Stable ZnO Thin  
357 Film Transistors by Fast Open Air Atomic Layer Deposition. *Appl. Phys. Lett.* **2008**, *92* (19). DOI:  
358 10.1063/1.2924768.
- 359 (28) Muñoz-Rojas, D.; Sun, H.; Iza, D. C.; Weickert, J.; Chen, L.; Wang, H.; Schmidt-Mende, L.;  
360 MacManus-Driscoll, J. L. High-Speed Atmospheric Atomic Layer Deposition of Ultra Thin

- 361 Amorphous TiO<sub>2</sub> Blocking Layers at 100 °C for Inverted Bulk Heterojunction Solar Cells. *Prog.*  
362 *Photovoltaics Res. Appl.* **2013**, 21 (4), 393–400. DOI: 10.1002/PIP.2380.
- 363 (29) Levy David H. Process for Atomic Layer Deposition. US-7413982-B2, **2008**.
- 364 (30) de la Huerta, C. A. M.; Nguyen, V. H.; Sekkat, A.; Crivello, C.; Toldra-Reig, F.; Veiga, P. B.;  
365 Quessada, S.; Jimenez, C.; Muñoz-Rojas, D. Gas-Phase 3D Printing of Functional Materials. *Adv.*  
366 *Mater. Technol.* **2020**, 5, 2000657. DOI: 10.1002/admt.202000657.
- 367 (31) Muñoz-Rojas, D.; Weber, M.; Va L L É E, C.; Crivello, C.; Sekkat, A.; Toldra-Reig, F.; Bechelany,  
368 M. Nanometric 3D Printing of Functional Materials by Atomic Layer Deposition. *Adv. Addit.*  
369 *Manuf.; IntechOpen*, **2022**. DOI: 10.5772/INTECHOPEN.101859.
- 370 (32) Ommen, J. R. van; Kooijman, D.; Niet, M. de; Talebi, M.; Goulas, A. Continuous Production of  
371 Nanostructured Particles Using Spatial Atomic Layer Deposition. *J. Vac. Sci. Technol. A Vacuum,*  
372 *Surfaces, Film.* **2015**, 33 (2), 021513. DOI: 10.1116/1.4905725.
- 373 (33) Li, J.; Pumera, M. 3D Printing of Functional Microrobots. *Chem. Soc. Rev.* **2021**, 50 (4), 2794–  
374 2838. DOI: 10.1039/D0CS01062F.
- 375 (34) Browne, M. P.; Plutnar, J.; Pourrahimi, A. M.; Sofer, Z.; Pumera, M. Atomic Layer Deposition as  
376 a General Method Turns Any 3D-Printed Electrode into a Desired Catalyst: Case Study in  
377 Photoelectrochemistry. *Adv. Energy Mater.* **2019**, 9 (26), 1900994.
- 378 (35) Ng, S.; Zazpe, R.; Rodriguez-Pereira, J.; Michalička, J.; Macak, J. M.; Pumera, M. Atomic Layer  
379 Deposition of Photoelectrocatalytic Material on 3D-Printed Nanocarbon Structures. *J. Mater.*  
380 *Chem. A* **2021**, 9 (18), 11405–11414.
- 381 (36) Nguyen, V. H.; Resende, J.; Jiménez, C.; Deschanvres, J.-L.; Carroy, P.; Muñoz, D.; Bellet, D.;  
382 Muñoz-Rojas, D. Deposition of ZnO Based Thin Films by Atmospheric Pressure Spatial Atomic  
383 Layer Deposition for Application in Solar Cells. *J. Renew. Sustain. Energy* **2017**, 9 (2), 021203.  
384 DOI: 10.1063/1.4979822.
- 385 (37) Nguyen, V. H.; Sekkat, A.; Masse De La Huerta, C. A.; Zoubian, F.; Crivello, C.; Rubio-Zuazo, J.;  
386 Rubio-Zuazo, J.; Jaffal, M.; Bonvalot, M.; Vallée, C.; Aubry, O.; Rabat, H.; Hong, D.; Muñoz-  
387 Rojas, D. Atmospheric Plasma-Enhanced Spatial Chemical Vapor Deposition of SiO<sub>2</sub> Using  
388 Trivinylmethoxysilane and Oxygen Plasma. *Chem. Mater.* **2020**, 32 (12), 5153–5161. DOI:  
389 10.1021/ACS.CHEMMATER.0C01148.
- 390 (38) de la Huerta, C. M.; Nguyen, V. H.; Dedulle, J. M.; Bellet, D.; Jiménez, C.; Muñoz-Rojas, D.  
391 Influence of the Geometric Parameters on the Deposition Mode in Spatial Atomic Layer  
392 Deposition: A Novel Approach to Area-Selective Deposition. *Coatings* **2018**, 9 (1), 5. DOI:  
393 10.3390/COATINGS9010005.
- 394 (39) Nguyen, V. H.; Sekkat, A.; Jiménez, C.; Muñoz, D.; Bellet, D.; Muñoz-Rojas, D. Impact of  
395 Precursor Exposure on Process Efficiency and Film Properties in Spatial Atomic Layer Deposition.  
396 *Chem. Eng. J.* **2021**, 403, 126234. DOI: 10.1016/j.cej.2020.126234.
- 397 (40) Weber, M.; Drobek, M.; Rebière, B.; Charmette, C.; Cartier, J.; Julbe, A.; Bechelany, M. Hydrogen  
398 Selective Palladium-Alumina Composite Membranes Prepared by Atomic Layer Deposition. *J.*  
399 *Memb. Sci.* **2020**, 596, 117701. DOI: 10.1016/j.memsci.2019.117701.
- 400 (41) Weber, M.; Bechelany, M. Combining Nanoparticles Grown by ALD and MOFs for Gas  
401 Separation and Catalysis Applications. *Pure Appl. Chem.* **2020**, 92 (2), 213–222. DOI:  
402 10.1515/PAC-2019-0109.
- 403 (42) Vøllestad, E.; Strandbakke, R.; Tarach, M.; Catalán-Martínez, D.; Fontaine, M. L.; Beeff, D.;



- 404 Clark, D. R.; Serra, J. M.; Norby, T. Mixed Proton and Electron Conducting Double Perovskite  
405 Anodes for Stable and Efficient Tubular Proton Ceramic Electrolysers. *Nat. Mater.* **2019**, *18* (7),  
406 752–759. DOI: 10.1038/s41563-019-0388-2.
- 407 (43) Morejudo, S. H.; Zanón, R.; Escolástico, S.; Yuste-Tirados, I.; Malerød-Fjeld, H.; Vestre, P. K.;  
408 Coors, W. G.; Martínez, A.; Norby, T.; Serra, J. M.; Kjølseth, C. Direct Conversion of Methane to  
409 Aromatics in a Catalytic Co-Ionic Membrane Reactor. *Science* (80-. ). **2016**, *353* (6299), 563–566.  
410 DOI: 10.1126/SCIENCE.AAG0274.
- 411 (44) Tan, X. Y.; Yin, W. N.; Meng, B.; Meng, X. X.; Yang, N. T.; Ma, Z. F. Preparation of Electrolyte  
412 Membranes for Micro Tubular Solid Oxide Fuel Cells. *Sci. China Ser. B Chem.* **2008**, *51*  
413 (9), 808–812. DOI: 10.1007/S11426-008-0068-6.
- 414 (45) Zhu, L.; O’Hayre, R.; Sullivan, N. P. High Performance Tubular Protonic Ceramic Fuel Cells via  
415 Highly-Scalable Extrusion Process. *Int. J. Hydrogen Energy* **2021**, *46* (54), 27784–27792. DOI:  
416 10.1016/J.IJHYDENE.2021.06.018.
- 417 (46) Agbede, O. O.; Hellgardt, K.; Kelsall, G. H. Electrical Conductivities and Microstructures of LSM,  
418 LSM-YSZ and LSM-YSZ/LSM Cathodes Fabricated on YSZ Electrolyte Hollow Fibres by Dip-  
419 Coating. *Mater. Today Chem.* **2020**, *16*, 100252. DOI: 10.1016/J.MTCHEM.2020.100252.
- 420 (47) Kleiminger, L.; Li, T.; Li, K.; Kelsall, G. H. Syngas (CO-H<sub>2</sub>) Production Using High Temperature  
421 Micro-Tubular Solid Oxide Electrolysers. *Electrochim. Acta* **2015**, *179*, 565–577. DOI:  
422 10.1016/J.ELECTACTA.2015.07.062.
- 423 (48) Morales, M.; Laguna-Bercero, M. A. Microtubular Solid Oxide Fuel Cells Fabricated by Gel-  
424 Casting: The Role of Supporting Microstructure on the Mechanical Properties. *RSC Adv.* **2017**, *7*  
425 (29), 17620–17628. DOI: 10.1039/C7RA01259D.
- 426 (49) Kherad, R.; Dodangei, S.; Moussavi, S. H.; Ghatee, M. Characterization of Anode Supported  
427 Micro-Tubular Solid Oxide Fuel Cells Prepared by Successive Non-Aqueous Electrophoretic  
428 Deposition. *J. Electroceramics* **2021**, *1*, 1–7. DOI: 10.1007/S10832-021-00272-5.
- 429 (50) Li, Y.; Chen, L.; Zhang, L.; Xia, C. Millimeter Tubular Solid Oxide Electrolysis Cells with  
430 Modified Asymmetric Hydrogen Electrode. *Int. J. Hydrogen Energy* **2016**, *41* (10), 5209–5214.  
431 DOI: 10.1016/J.IJHYDENE.2016.01.103.
- 432 (51) Tan, Z.; Ishihara, T. Effect of Ni-Based Cathodic Layer on Intermediate Temperature Tubular  
433 Electrolysis Cell Using LaGaO<sub>3</sub>-Based Electrolyte Thin Film. *JPhys Energy* **2020**, *2* (2), 024004.  
434 DOI: 10.1088/2515-7655/ab6f4b.
- 435 (52) Gong, T.; Huang, Y.; Qin, L.; Zhang, W.; Li, J.; Hui, L.; Feng, H. Atomic Layer Deposited  
436 Palladium Nanoparticle Catalysts Supported on Titanium Dioxide Modified MCM-41 for Selective  
437 Hydrogenation of Acetylene. *Appl. Surf. Sci.* **2019**, *495*, 143495. DOI:  
438 10.1016/J.APSUSC.2019.07.237.
- 439 (53) Chen, R.; Qu, K.; Li, J.; Zhu, P.; Duan, C.; Zhang, J.; Li, X.; Liu, X.; Yang, Z. Ultrathin Zirconia  
440 Passivation and Stabilization of Aluminum Nanoparticles for Energetic Nanomaterials via Atomic  
441 Layer Deposition. *ACS Appl. Nano Mater.* **2018**, *1* (10), 5500–5506. DOI:  
442 10.1021/acsanm.8b01005.
- 443 (54) Park, J.; Lee, Y.; Chang, I.; Cho, G. Y.; Ji, S.; Lee, W.; Cha, S. W. Atomic Layer Deposition of  
444 Yttria-Stabilized Zirconia Thin Films for Enhanced Reactivity and Stability of Solid Oxide Fuel  
445 Cells. *Energy* **2016**, *116*, 170–176. DOI: 0.1016/J.ENERGY.2016.09.094.
- 446 (55) Oh, S.; Park, J.; Shin, J. W.; Yang, B. C.; Zhang, J.; Jang, D. Y.; An, J. High Performance Low-

- 447 Temperature Solid Oxide Fuel Cells with Atomic Layer Deposited-Yttria Stabilized Zirconia  
448 Embedded Thin Film Electrolyte. *J. Mater. Chem. A* **2018**, *6* (17), 7401–7408. DOI:  
449 10.1039/C7TA10678E.
- 450 (56) Fan, L.; Zhu, B.; Su, P. C.; He, C. Nanomaterials and Technologies for Low Temperature Solid  
451 Oxide Fuel Cells: Recent Advances, Challenges and Opportunities. *Nano Energy* **2018**, *45*, 148–  
452 176. DOI: 10.1016/j.nanoen.2017.12.044.
- 453 (57) Pessoa, R. S.; Fraga, M. A.; Chiappim, W.; Maciel, H. S. Exploring the Properties and Fuel Cell  
454 Applications of Ultrathin Atomic Layer Deposited Metal Oxide Films. *Emerg. Mater. Energy*  
455 *Convers. Storage*, Cheong, K.Y.; Impellizzeri, G.; Fraga, M.A.; Eds.; El Sevier, London, **2018**,  
456 83–114. DOI: 10.1016/B978-0-12-813794-9.00003-X.
- 457 (58) Shim, J. H.; Chao, C. C.; Huango, H.; Prinz, F. B. Atomic Layer Deposition of Yttria-Stabilized  
458 Zirconia for Solid Oxide Fuel Cells. *Chem. Mater.* **2007**, *19* (15), 3850–3854. DOI:  
459 10.1021/cm070913t.
- 460 (59) Shim, J. H.; Park, J. S.; An, J.; Gür, T. M.; Kang, S.; Prinz, F. B. Intermediate-Temperature Ceramic  
461 Fuel Cells with Thin Film Yttrium-Doped Barium Zirconate Electrolytes. *Chem. Mater.* **2009**, *21*  
462 (14), 3290–3296. DOI: 10.1021/cm900820p.
- 463 (60) Park, J. S.; Kim, Y. B.; Shim, J. H.; Kang, S.; Gür, T. M.; Prinz, F. B. Evidence of Proton Transport  
464 in Atomic Layer Deposited Yttria-Stabilized Zirconia Films. *Chem. Mater.* **2010**, *22* (18), 5366–  
465 5370. DOI: 10.1021/cm1017536.
- 466 (61) Konda, A.; Rau, A.; Stoller, M. A.; Taylor, J. M.; Salam, A.; Pribil, G. A.; Argyropoulos, C.; Morin,  
467 S. A. Soft Microreactors for the Deposition of Conductive Metallic Traces on Planar, Embossed,  
468 and Curved Surfaces. *Adv. Funct. Mater.* **2018**, *28* (40). DOI: 10.1002/ADFM.201803020.
- 469 (62) Tian, M.; Su, Y.; Zheng, H.; Pei, G.; Li, G.; Riffat, S. A Review on the Recent Research Progress  
470 in the Compound Parabolic Concentrator (CPC) for Solar Energy Applications. *Renew. Sustain.*  
471 *Energy Rev.* **2018**, *82*, 1272–1296. DOI: 10.1016/J.RSER.2017.09.050.
- 472 (63) Ko, H. C.; Stoykovich, M. P.; Song, J.; Malyarchuk, V.; Choi, W. M.; Yu, C. J.; Geddes, J. B.;  
473 Xiao, J.; Wang, S.; Huang, Y.; Rogers, J. A. A Hemispherical Electronic Eye Camera Based on  
474 Compressible Silicon Optoelectronics. *Nat.* **2008**, *454* (7205), 748–753. DOI:  
475 10.1038/nature07113.

476

477

478

479

480

481

482

483

484

485

486

487

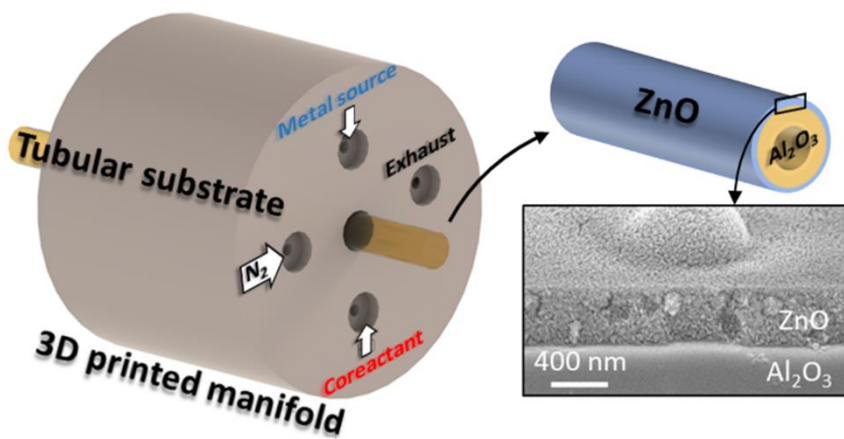
488

489

490

491

For Table of Contents Use Only



492

493 3D-printed spatial atomic layer deposition gas manifold for coating of non-planar substrates like tubular  
494 samples

495